

Chiral plasmons without magnetic field

Justin C. W. Song¹ and Mark S. Rudner²

¹ *Walter Burke Institute for Theoretical Physics and Institute for Quantum Information and Matter, California Institute of Technology, Pasadena, CA 91125 USA and*

² *Center for Quantum Devices and Niels Bohr International Academy, Niels Bohr Institute, University of Copenhagen, 2100 Copenhagen, Denmark*

We predict a new class of collective excitations – chiral Berry plasmons (CBPs) – occurring generically in interacting metallic systems with nonzero Berry flux. Such systems include e.g., anomalous Hall metals and optically-pumped valley polarized 2D Dirac materials such as transition metal dichalcogenides. In this context, a unique situation arises wherein the interplay between Bloch band Berry curvature and interactions yields chiral collective modes at zero magnetic field. CBP modes are confined to system boundaries, even in the absence of topological edge states, with chirality manifested in split energy dispersions for oppositely directed plasmon waves. Directly dependent on Berry flux, plasmon wave vector, and interaction strength, the mode splitting is tunable and can be large. CBPs yield clear experimental signatures such as split optical absorption peaks in a disk geometry, as well as frequency selective uni-directional propagation along the edge. Realization of CBPs will offer a new paradigm for magnetic field-free, sub-wavelength optical non-reciprocity, as well as sensitive all-optical diagnostics of topological bands.

Chirality in electronic systems is commonly associated with the presence of an applied magnetic field. However, materials exhibiting chirality in the absence of a magnetic field have recently gained prominence. These include metals exhibiting anomalous- [1] and quantum anomalous- [2–6] Hall effects, as well as out-of-equilibrium systems such as MoS₂ with light-induced valley polarization, where a charge Hall effect was recently demonstrated [7]. In each case, zero-field chirality arises from Bloch band Berry curvature, a fundamental property of Bloch eigenstates that dramatically affects single-particle electronic motion and material responses [1, 8, 9].

Here we show that Berry curvature can work in concert with interactions, leading to new types of *collective modes* in two-dimensional (2D) metallic systems with non-vanishing Berry flux (i.e., net Berry curvature), \mathcal{F} . In particular, \mathcal{F} gives rise to *chiral* plasmonic excitations — propagating charge density waves with split dispersion for oppositely directed modes — in the absence of a magnetic field (Fig. 1a). We refer to these collective modes as “chiral Berry plasmons” (CBPs). Notably, these chiral modes are localized to the edge of the 2D metal, even in the absence of topological edge states (Fig. 1b), and exhibit a rich phenomenology (see below).

The intrinsic chirality of CBPs starkly contrasts with that achieved via cyclotron motion of charged particles in a magnetic field. In the latter case, chirality arises via the Lorentz force and gives rise to conventional magnetoplasmons [10–13]. There, the cyclotron frequency, $\hbar\omega_c = \hbar eB/m$ [14], determines the constant splitting between magnetoplasmon modes of opposite chirality, which can be of order a few meV for accessible field strengths. In contrast, chirality in CBPs arises from the combined action of plasmonic self-generated electric fields and the anomalous velocity of Bloch electrons, the phase space *dual* to the Lorentz force. This combination

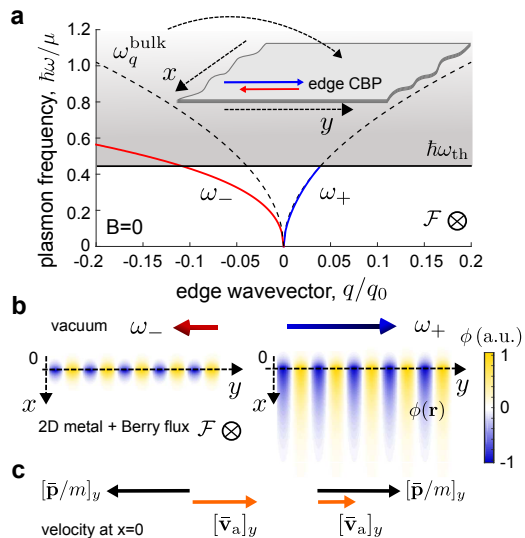


FIG. 1: **Chiral Berry plasmons (CBPs) at zero magnetic field.** **a)** CBPs are manifested along the edges of a 2D metal with non-vanishing Berry flux, \mathcal{F} (inset). Counter-propagating modes exhibit a split dispersion, $\omega_{\pm}(q)$, with the splitting $\Delta\omega(q) = \omega_+(q) - \omega_-(q)$ increasing with wave vector q along the edge. Above a threshold frequency $\hbar\omega_{\text{th}}$, the fast mode ω_+ merges with bulk plasmon modes (dashed line), leaving only the *single unidirectional mode* ω_- propagating on the edge (shaded region). **b)** The CBP electric potential $\phi(\mathbf{r})$ is localized near system edges [shown for a half-plane: metal ($x > 0$), vacuum ($x < 0$)]. The fast mode ω_+ extends significantly further into the metallic bulk than the ω_- mode. **c)** The CBP velocity field near the edge ($x = 0$) is comprised of conventional, $[\bar{\mathbf{p}}/m]_y$ (black), and anomalous, $[\bar{\mathbf{v}}_a]_y$ (orange), components, see Eqs. (1) and (2) [only relative signs are shown for illustration]. Depending on propagation direction, $[\bar{\mathbf{p}}/m]_y$ and $[\bar{\mathbf{v}}_a]_y$ are parallel (anti-parallel), giving faster (slower) modes, see text below Eq. (2). Parameter values used for a) and b): $\mathcal{F} = 0.4$, and $a_0 = 5$, and $q/q_0 = 0.03$ (panel b), with q_0 a material dependent scale [see text and Eq. (5)].

makes the CBP mode splitting directly sensitive to plas-

mon wavelength, the Berry flux, and interaction strength, in contrast to magnetoplasmon splittings which only depend on magnetic field[12, 15] [39]. As a result, for short wavelengths and unscreened interactions, large splittings $\hbar\Delta\omega \approx 10-100$ meV can be achieved [see Eq. (3) below].

We expect CBPs to be manifested in a wide variety of magnetic materials exhibiting anomalous Hall effects, wherein time reversal symmetry (TRS) breaking is encoded in the band Berry curvature. Intriguingly (and perhaps surprisingly), CBPs can also be realized in *non-magnetic* materials. We predict that a range of gapped Dirac materials, e.g., transition metal dichalcogenides and graphene/hBN, can also host CBPs when valley polarized (e.g., via optical pumping). In both cases CBPs are characterized by clear optical signatures such as split peaks in optical absorption.

From a technological perspective, CBPs in non-magnetic materials are particularly appealing since they provide an entirely new platform for achieving a range of magneto-optical effect analogues that are magnetic field-free, and “on demand.” A prime example is optical non-reciprocity [17], which is central for optical device components e.g., optical isolators and circulators. Above a threshold frequency (ω_{th} , see shaded area in Fig. 1a), the single unidirectionally propagating mode ω_- allows for chiral transport of light via coupling to CBPs. Such CBP mediated waveguides provide a novel paradigm for deep sub wavelength [18–20], linear, and magnetic field free strong non-reciprocity, crucial for miniaturizing optical components.

Self-Induced Anomalous Velocity - The origin of CBPs in two dimensions can be understood, in the hydrodynamic limit, via Euler equations for electron density $n(\mathbf{r}, t)$ [21]:

$$\partial_t n(\mathbf{r}, t) + \nabla \cdot \bar{\mathbf{v}}(\mathbf{r}, t) = 0, \quad (1a)$$

$$\partial_t \bar{\mathbf{p}}(\mathbf{r}, t) - n(\mathbf{r}, t) e \nabla \phi(\mathbf{r}, t) + \nabla_j \bar{\sigma}_{ij} = 0, \quad (1b)$$

where $\bar{\mathbf{v}}(\mathbf{r}, t)$ and $\bar{\mathbf{p}}(\mathbf{r}, t)$ are the velocity and momentum density fields, $\bar{\sigma}_{ij}$ is the stress density tensor of the electron fluid, $\phi(\mathbf{r})$ is the scalar electric potential, and $-e < 0$ is the electron charge. In order to fully specify the dynamics, Eq. (1) must be supplemented by a set of *constitutive relations* which relate velocity, momentum, density, stress density, and the electric potential. Plasmons emerge from Eq. (1) as self-sustained collective oscillations of $n(\mathbf{r}, t)$, with the potential $\phi(\mathbf{r}, t) = \int d^2 \mathbf{r}' W(\mathbf{r}, \mathbf{r}') \delta n(\mathbf{r}', t)$ generated by the plasmon’s density oscillations $\delta n = n(\mathbf{r}, t) - n_0$. Here n_0 is the average carrier density, and $W(\mathbf{r}, \mathbf{r}')$ is the Coulomb interaction.

As we argue, in the presence of Berry curvature, the constitutive relations take on an anomalous character. This can be seen by starting with the quasiparticle semi-classical equations of motion [8], $\mathbf{v}_p = \frac{\partial \varepsilon_p}{\partial \mathbf{p}} + \frac{1}{\hbar} \dot{\mathbf{p}} \times \Omega(\mathbf{p})$, $\dot{\mathbf{p}} = e \nabla \phi(\mathbf{r})$, where $\mathbf{v}_p = \dot{\mathbf{r}}$ is the quasiparticle velocity and ε_p and $\Omega(\mathbf{p}) = \Omega(\mathbf{p}) \hat{\mathbf{z}}$ are the Bloch band disper-

sion and Berry curvature, respectively [40]. The corresponding hydrodynamic fields are found from these relations and the phase space density $f_i(\mathbf{r}, \mathbf{p}, t)$ by summing over all momentum \mathbf{p} and bands $\{i\}$, $\bar{\mathcal{O}}(\mathbf{r}, t) = \sum_{\mathbf{p}, i} \mathcal{O} f_i(\mathbf{r}, \mathbf{p}, t)$ [22]. This gives:

$$\bar{\mathbf{v}}(\mathbf{r}, t) = \frac{\bar{\mathbf{p}}(\mathbf{r}, t)}{m} + \bar{\mathbf{v}}_a(\mathbf{r}, t), \quad \bar{\mathbf{v}}_a = \frac{e \mathcal{F}}{\hbar} [(\nabla \phi) \times \hat{\mathbf{z}}], \quad (2)$$

where $\mathcal{F} = \sum_{\mathbf{p}, i} \Omega_i(\mathbf{p}) f_i^0(\mathbf{p})$ is the (dimensionless) Berry flux, with $f_i^0(\mathbf{p})$ the equilibrium band occupancy. In addition to the conventional first term, which governs the behavior of ordinary plasmons, $\bar{\mathbf{v}}(\mathbf{r}, t)$ in Eq. (2) exhibits a self-induced anomalous velocity component $\bar{\mathbf{v}}_a$ that yields chirality as shown in Fig. 1. Note that the mass m appearing in Eq. (2) is the *plasmon mass*, which characterizes the collective motion of the Fermi sea [23].

CBP chirality can be intuitively understood by considering the velocity density $\bar{\mathbf{v}}(\mathbf{r}, t)$ along the sample boundary (a more complete treatment is given below). For example, at a boundary defined by $x = 0$ the net velocity must be oriented along $\hat{\mathbf{y}}$. The plasmon’s plane wave potential profile $\phi(\mathbf{r}, t) = \phi(x) e^{i\omega t - iqy}$ (Fig. 1b) sets up a spatiotemporally oscillating velocity field featuring a conventional component, $[\bar{\mathbf{p}}/m]_y$, and an anomalous component, $[\bar{\mathbf{v}}_a]_y$ (see Fig. 1c). Importantly, the anomalous component depends on the electric field *perpendicular* to the edge (the x -direction), see Eq. (2), while the conventional component depends on the electric field *along* the edge, Eq. (1). As a result, depending on the direction of propagation along the edge, the normal and anomalous components may be parallel or anti-parallel, yielding fast and slow modes ω_+ and ω_- , respectively (see Fig. 1c).

Crucially, $\bar{\mathbf{v}}_a$ depends directly on the self-generated electric field $-\nabla \phi(\mathbf{r})$. Consequently, the magnitude of the splitting is governed by the wave vector q and the strength of Coulomb interactions. We emphasize, however, that CBPs are *linear*, with the mode splitting $\Delta\omega$ being independent of the magnitude of ϕ . Estimating $\hbar[\bar{\mathbf{v}}_a]_y \approx e \mathcal{F} \partial_x \phi(x = 0) \approx 2\pi e^2 \delta n / \kappa$, where $\delta n \sim e^{i\omega t - iqy}$ is a plane wave, and comparing with Eq. (1a), we estimate the CBP splitting:

$$\hbar \Delta\omega = \hbar(\omega_+ - \omega_-) \approx \hbar v_a |q| \approx \frac{2\pi e^2}{\kappa} \mathcal{F} |q|. \quad (3)$$

Here we have used the 2D Coulomb potential $W(\mathbf{q}) = 2\pi e^2 / (|\mathbf{q}| \kappa)$, where κ is the background dielectric constant. Taking $\mathcal{F} = 1$ and $\kappa = 1$ yields $\hbar \Delta\omega \approx 10 - 100$ meV for $q = 1 - 10 \mu\text{m}^{-1}$. The appearance of e^2/κ on the right hand side of Eq. (3) signals the crucial role of interactions in determining the CBP splitting. Our calculations below support these estimates, revealing the exceptionally wide splitting windows achievable with CBPs.

Chiral Edge Berry Plasmons - We now analyze the collective CBP motion described by Eq. (1), treating

the electric potential ϕ self-consistently. In so doing, we first note that CBPs only arise in systems with boundaries. This can be seen by analyzing the force equation for charge density in an infinite bulk. Noting that $\nabla \cdot \bar{\mathbf{v}}_a \propto \partial_x \partial_y \phi(\mathbf{r}) - \partial_y \partial_x \phi(\mathbf{r}) = 0$, and applying ∂_t to the charge continuity equation in Eq. (1), we find

$$[-\partial_t^2 + \frac{\mu}{2m} \nabla^2] \delta n - \frac{n_0 e}{m} \nabla^2 \phi = 0. \quad (4)$$

In writing Eq. (4) we have used Eq. (2), along with the constitutive relation for stress density (in the degenerate limit [22]) $\bar{\sigma}_{ij} = \frac{\mu}{2} \delta n \delta_{ij}$, and kept terms up to linear order in δn . Here μ is the chemical potential (measured from the bottom of the band), which enters through the distribution $f_i(\mathbf{r}, \mathbf{p}, t)$.

Importantly, \mathcal{F} is absent in Eq. (4) and thus has no effect on the (gapless) bulk plasmon dispersion:

$$(\hbar \omega_{\mathbf{q}}^{\text{bulk}} / \mu)^2 = (\hbar \omega_{\mathbf{q}} / \mu)^2 + (|\mathbf{q}| / q_0)^2, \quad \frac{\hbar \omega_{\mathbf{q}}}{\mu} = a_0 \frac{|\mathbf{q}|}{q_0}. \quad (5)$$

Here, dimensionless $a_0 = 4\pi e^2 n_0 / (\kappa \mu q_0)$ characterizes the Coulomb interactions, $W(\mathbf{r}, \mathbf{r}') = -\frac{e}{\kappa |\mathbf{r} - \mathbf{r}'|}$, and $q_0 = (2m\mu/\hbar^2)^{1/2}$ is an inverse characteristic length [22]. In contrast, bulk magnetoplasmons are *gapped* due to cyclotron motion [11–13]. For a sense of scale, graphene has $q_0 = \sqrt{2}\mu/(v_F \hbar) \approx (2.15 \times 10^4) \times (\mu[\text{meV}]) \text{ cm}^{-1}$, and $a_0 = 6.2$; see SOI for detailed estimates.

Close to a boundary, the situation is dramatically altered: Berry flux leads to the emergence of *chiral edge plasmons*, one-dimensional chiral analogues of surface plasmons [15, 24]. For an infinite half-plane, $n(\mathbf{r}, t) = n(\mathbf{r}, t)\Theta(x)$, edge CBPs are *localized* in x and propagate as plane waves $\sim e^{i\omega t - iqy}$ along y (see Fig. 1b).

We now seek edge-confined solutions of Eq. (4), solving for the electric potentials $\phi_>$ and $\phi_<$ inside ($x > 0$) and outside ($x < 0$) the sample, respectively, with $\phi(x) = \int dx' W_q(x - x') \delta n(x')$. For an isolated system, the bare Coulomb kernel $W_q(x)$ yields highly non-local integro-differential equations. Here we adopt a simplified local kernel approach developed in Refs. [15, 24] that captures the essential physics via simple relations for ϕ , $(\partial_x^2 - 2q^2)\phi_> = 4\pi e|q|\delta n/\kappa$ and $(\partial_x^2 - 2q^2)\phi_< = 0$ [15, 24], while mimicking interactions in an isolated system. This method successfully describes edge magnetoplasmons in 2D systems such as electrons on liquid helium [12], and graphene [25]. Specific background screening geometries can be considered via other choices of $W_q(x)$. However, we expect our qualitative conclusions to generally hold.

Near the boundary $x = 0$, the localized modes go as

$$\phi_< = \phi_0 e^{\gamma_0 x}, \quad \phi_> = \phi_1 e^{-\gamma_1 x} + \phi_2 e^{-\gamma_2 x}. \quad (6)$$

The decay constants $\gamma_0(q)$ and $\gamma_{1,2}(q)$ are determined by Eq. (4) and the approximate kernel above. We find $\gamma_0 = \sqrt{2}|q|$, while $\gamma_{1,2}$ are given by the positive roots

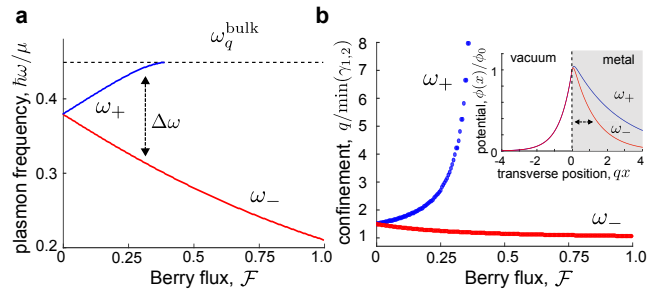


FIG. 2: **Chiral Berry plasmons at the boundary of a half plane.** **a**) The CBP frequency splitting increases with increasing Berry flux, \mathcal{F} . Parameter values used are as in Fig. 1, but with $|q|/q_0 = 0.04$. **b**) CBP confinement length to the edge, $[\min(\gamma_{1,2})]^{-1}$, of ω_+ and ω_- , see Eq. (6), for increasing \mathcal{F} . For large \mathcal{F} , the confinement length for the ω_+ mode diverges, indicating that it joins the bulk, while the ω_- mode becomes more confined to the edge. (inset) EM profile shown for $\mathcal{F} = 0.25$, exhibiting the confinement of the ω_{\pm} modes to the edge.

of the quartic equation: $\gamma^4 - \gamma^2 [3q^2 + \frac{2m}{\mu} (2\omega_{\mathbf{q}}^2 - \omega^2)] + 2q^2 [q^2 + \frac{2m}{\mu} (\omega_{\mathbf{q}}^2 - \omega^2)] = 0$ [15].

The constants ϕ_0 and $\phi_{1,2}$ appearing in Eq. (6) are fixed by enforcing appropriate boundary conditions for ϕ and electron density. Here we demand that ϕ and $\partial_x \phi$ must be continuous across the boundary, while \bar{v}_x must vanish there to ensure that the electron liquid stays inside the metal. Importantly, the last of these conditions is sensitive to the anomalous velocity \bar{v}_a .

Solving for ϕ satisfying the above boundary conditions, we obtain edge CBPs shown in Figs. 1 and 2 (see SOI). For $\mathcal{F} \neq 0$ this yields two chiral modes that are localized close to the edge, with distinct frequencies ω_{\pm} . The modes ω_+ and ω_- propagate as waves in opposite directions along the edge (Fig. 1a), as well as \mathcal{F} (Fig. 2a). The splitting between modes grows with q and \mathcal{F} , since $\bar{v}_a = e\nabla\phi \times \mathcal{F}/\hbar$ [see Eq. (2)]. In particular, large q produces large self-induced electric fields, leading to large \bar{v}_a and hence a large CBP splitting. This behavior sharply contrasts that of magnetoplasmons, which have a q -independent splitting given by the cyclotron frequency [12, 14, 15, 24]. As a result, far larger splittings, arising from interactions, can be achieved for CBPs.

Interestingly, for large enough q and/or \mathcal{F} , the ω_+ mode (blue line in Figs. 1a and 2a) merges with the bulk plasmon mode ω_q^{bulk} (dashed line). As this mode merges with the bulk, its potential profile ceases to be localized along the edge. This is shown by a diverging confinement length of the EM potential, $[\min(\gamma_{1,2})]^{-1}$, see Fig. 2b. In contrast, ω_- stays far from the bulk dispersion, yielding a potential (and electric field) tightly confined to the edge. An estimate of the frequency threshold ω_{th} above which ω_+ merges with the bulk can be obtained

by comparing the splitting in Eq. (3) with the bulk plasmon frequency [Eq. (5)]; it can also be read off Fig. 1a, 2a. Keeping only the first term in Eq. (5), we obtain $\omega_{\text{th}} \approx \hbar n_0/m\mathcal{F}$. For a Dirac system with N fermion flavors, we obtain $\hbar\omega_{\text{th}} \approx N\mu/4\pi\mathcal{F} = 30 - 100$ meV (for typical $\mu = 100 - 300$ meV, and setting $\mathcal{F} = 1$, $N = 4$).

Conservation of ω and q along the edge protect the ω_- mode from coupling to bulk 2D plasmons. Scattering processes that relax q contribute to propagation losses. However, the tight edge confinement of the ω_- mode suppresses its electric field in the bulk regions, hence suppressing its coupling to bulk plasmon modes. Therefore, above the threshold ω_{th} (gray region in Fig. 1a), the single, well-defined, ω_- mode propagates unidirectionally along the edge, allowing for strong non-reciprocal propagation of hybrid CBP polaritons without magnetic field.

Experimental Signatures of CBPs - Strong plasmon mediated light-matter interactions [18–20] make optics an ideal means of probing/controlling CBPs. Photon coupling to plasmons with gapless dispersion (e.g. 2D plasmons, and CBPs here) can be achieved through strategies such as gratings, and prism geometries [18]. Observing unidirectional (non-reciprocal) propagation in such setups can reveal the existence of CBPs. For demonstration, we detail an alternative experimental probe: CBP-photon coupling in finite geometries, such as metallic disks, where dipolar plasmonic modes can dominate optical absorption [10, 18].

In metallic disks with finite \mathcal{F} , CBPs manifest as clockwise/anti-clockwise moving plasmonic dipole modes (Fig. 3a). These modes can be described via a simple oscillator model for the motion of the dipolar CBP center of mass (COM) coordinate [22], $\{\mathbf{x}\}$, where $\{\cdot\}$ denotes the COM average. Here $\{\mathbf{v}_a\} \approx \{e\nabla\phi\} \times \mathcal{F}$ (green arrow) gives rise to an intrinsic angular frequency ω_a of plasmons in a disk (orange arrow), which adds to (subtracts from) the plasmon frequency ω_0 to produce non-degenerate clockwise (anti clockwise) rotating modes (Fig. 3a); see detailed derivation in SOI. Here we have used \mathcal{F} pointing to positive $\hat{\mathbf{z}}$. A bosonic analogue for ultra cold atomic gases is discussed in Ref. [26].

With an a.c. probing electric field $E_i e^{i\omega t}$, the COM equations of motion are $(\partial_t^2 + A_{ij})\{\mathbf{x}_j\} = eE_i e^{i\omega t}$, where

$$\mathbf{A} = \begin{pmatrix} \omega_0^2 & \omega_a \partial_t \\ -\omega_a \partial_t & \omega_0^2 \end{pmatrix}, \quad \omega_a = \frac{\mathcal{F}\omega_0^2 m}{n_0 \hbar}. \quad (7)$$

Here $\omega_0(d)$ is the bare plasmon frequency in a disk of diameter d , in the absence of Berry curvature.

Writing the current density as $\mathbf{j} = n_0 e \partial_t \{\mathbf{x}\}$, we invert the COM equations of motion to obtain the optical absorption (real part of the longitudinal conductivity [22]). As shown in Fig. 3b, we find a split peak structure with

the dipolar CBP peaks given by the poles of Eq. (7):

$$\omega_{\pm}^{\text{disk}} = \sqrt{\omega_0^2 + \frac{\omega_a^2}{4}} \pm \frac{\omega_a}{2}, \quad \hbar\Delta\omega = \mathcal{F}\hbar\omega_* \approx \frac{9\mathcal{F}}{d[\mu\text{m}]} \text{ meV}, \quad (8)$$

where $\Delta\omega = \omega_+^{\text{disk}} - \omega_-^{\text{disk}} = \omega_a$, and $\hbar\omega_* = \omega_0^2 m/n_0$. On the right side, we have estimated $\omega_0^2 \approx 2\pi e^2 n_0 |\mathbf{q}|/m$, with $|\mathbf{q}| \approx 1/d$ (approximating the lowest lying plasmonic excitation in a disk) [41]. Importantly, $\Delta\omega$ depends on the disk size, d , a unique property of CBPs.

The tunable optical absorption split peak structure (via \mathcal{F} and d) in the absence of an applied magnetic field gives a clear experimental signature of CBPs. In plotting Fig. 3b, we have included the damping rate phenomenologically via $\partial_t^2 \rightarrow \partial_t^2 + \Gamma\partial_t$, yielding a Lorentzian lineshape with its half-width determined by Γ . Split peaks are clearly visible when $\hbar\Delta\omega \gtrsim \Gamma$, yielding peaks at $\omega_{\pm}^{\text{disk}}$. To give a sense of scale, we note a typical value $\Gamma \sim \text{few meV}$, see e.g. Ref. [27] where $\Gamma \approx 4$ meV was measured in graphene disks. Using $\Gamma/\omega_* = 0.25$ and taking $\mathcal{F} = 1$, clearly resolved $\omega_{\pm}^{\text{disk}}$ peaks can be resolved for disk sizes $d \lesssim 1 \mu\text{m}$ (Fig. 3b).

CBPs in Anomalous Hall Materials - We now discuss materials where CBPs can be realized. We predict that metallic systems with non-vanishing \mathcal{F} will host CBPs. Finite \mathcal{F} requires broken time reversal symmetry, and may arise in magnetically ordered ground states, or out-of-equilibrium non-magnetic systems (see below). The former includes magnetically doped semiconducting quantum wells (see e.g., Ref. [28], where $\mathcal{F} \approx 1/2$ was predicted), and magnetic topological insulators [3–6].

As a concrete example, we examine the magnetically doped topological insulator, chromium doped thin-film $(\text{Bi},\text{Sb})_2\text{Te}_3$, which was recently experimentally realized [5]. When moderately doped with electrons or holes, we estimate that $\mathcal{F} \sim 1$ can be achieved based on the measured anomalous Hall conductivity $\sigma_{xy}^{B=0} \lesssim e^2/h$ [5]. This yields a large splitting $\Delta\omega \approx 10 - 100$ meV for short wavelength plasmons, see Eqs. (3) and (8). When probed in the disk geometry, we predict this system will yield two split absorption peaks in the absence of magnetic field.

Notably, chromium doped $(\text{Bi},\text{Sb})_2\text{Te}_3$ exhibits a quantum anomalous Hall (QAH) phase when the carrier density is fully depleted; when the Fermi energy lies in the gap, $\mathcal{F} = 1$. As a result, when we take $n_0 \rightarrow 0$ in Eq. (8) we find that a *single* CBP mode (ω_+) remains even at zero bulk density. This single mode describes collective excitations associated with the quantum anomalous Hall chiral edge state, and may be used to probe the QAH effect optically. Hence, absorption mediated by CBPs can serve as an optical probe of QAH phases.

“On-demand” CBPs in Non-Magnetic Materials - Intriguingly, finite \mathcal{F} can also be achieved in *non-magnetic* materials, without an applied magnetic field,

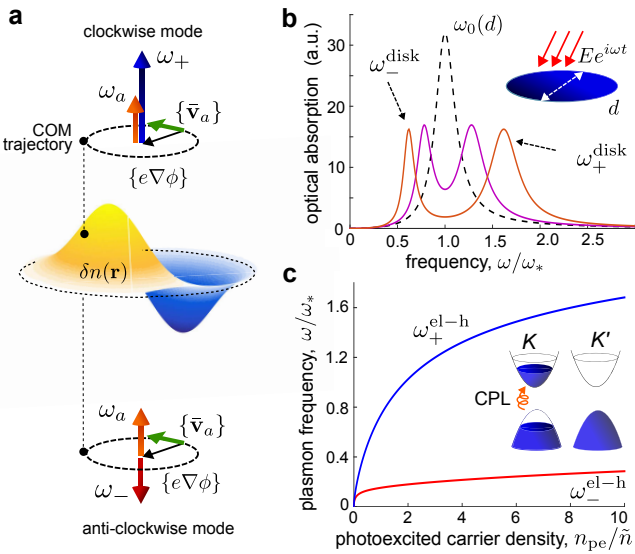


FIG. 3: Chiral Berry plasmons in a disk and in valley polarized gapped Dirac systems. **a.** Illustration of CBPs in a disk, showing clockwise/anticlockwise rotating dipole modes. The mode splitting arises from the intrinsic angular frequency, ω_a , induced by the combination of \mathcal{F} and the self-induced electric field. **b.** Optical absorption split peaks for dipolar CBPs in a disk (panel a) obtained by inverting Eq. (7) for $\mathcal{F} = 0, 0.5, 1.0$ (dashed black, purple, orange). Smaller disk sizes and/or larger \mathcal{F} produce larger splittings, see Eq. (8). Parameter values: $\omega_0/\omega_* = 1$ and $\Gamma/\omega_* = 0.25$. **c.** CBP dipole modes for valley polarized gapped Dirac systems, with $n_K = n_{pe}$, and $n_{K'} = 0$. Characteristic density is $\tilde{n} = \Delta^2/4\pi v_F^2 \hbar^2$. (inset) Valley polarization can be induced by above-gap circularly polarized light.

e.g., via pumping with circularly polarized light (see Fig. 3c inset). This protocol was used recently to induce a charge Hall effect in valley polarized MoS₂ [7], but can also be replicated in other gapped Dirac materials, e.g., WSe₂ [29], MoSe₂ [30], gapped graphene on hexagonal boron nitride (G/hBN) [31–33], and dual-gated bilayer graphene [34]. Note that the (neutral) excitons that may form in gapped Dirac materials feel zero net Berry curvature [35]; thus we do not expect them to exhibit chirality and focus only on the dynamics of excited free carriers.

Can CBPs exist in photoexcited systems? To analyze this, we focus on nominally time reversally invariant gapped Dirac materials. We model the valley dependent \mathcal{F} as [36]: $\mathcal{F}_{K,K'} = \tau_z N_s \frac{\tilde{n}^{1/2}}{2(n_{K,K'} + \tilde{n})^{1/2}} \text{sgn } \Delta$, where $n_{K,K'}$ are the valley carrier densities, $\tau_z = \mp$ for the K, K' valleys, $N_s = 2$ is the spin degeneracy, and $\tilde{n} = \Delta^2/4\pi v_F^2 \hbar^2$ gives a characteristic density scale. The bandgap is $2|\Delta|$. When $n_K = n_{K'}$, the total flux $\mathcal{F} = \mathcal{F}_K + \mathcal{F}'_K$ vanishes.

Interestingly, a non-vanishing net Berry flux \mathcal{F}_{pe} for the photoexcited system is achieved when $n_K \neq n_{K'}$ (Fig. 3c inset). We analyze the collective modes of the photo excited electron-hole system in the disk geometry

as above following Eq. (7) above. Accounting for \mathcal{F}_{pe} and the mutually attracting electron and hole populations we obtain two chiral CBP modes, $\omega_{\pm}^{el-h} = \sqrt{\omega_a^2 + 2\omega_0^2} \pm \omega_a$, see SOI. Estimating ω_0 as below Eq. (8), we obtain the ω_{\pm}^{el-h} curves shown in Fig. 3c with ω_* given by Eq. (8). Importantly, both modes have frequencies that vanish at zero photo excited carrier density. The mode splitting increases with photoexcited carrier density n_{pe} , and can reach sizable values for $n_{pe} \geq \tilde{n}$, reflecting \mathcal{F}_{pe} pumping.

To achieve observable splittings, photoexcited densities $n_{pe} \gtrsim \tilde{n}$ are required. For MoS₂, the large gap ($\Delta \approx 1$ eV) requires large $n_{pe} \gtrsim 10^{13} \text{ cm}^{-2}$. However, smaller gap systems, e.g., MoTe₂ ($2\Delta = 1$ eV [30]), offer significantly weaker n_{pe} requirements. Indeed, G/hBN [31–33] and dual-gated bilayer graphene [34], where $\Delta \approx 10 - 200$ meV, provide ideal venues to achieve maximal fluxes of $\mathcal{F} = 1$ and large CBP splittings $\Delta\omega$.

An alternative and promising strategy to achieve large CBP splittings is to stack m layers of gapped Dirac materials (e.g., TMDs) on top of each other, with no tunnel coupling between the layers [42]. Stacking achieves (i) larger photo excited carrier densities due to the increased absorption, and (ii) a larger maximal Berry flux (when $n_{pe} \gg \tilde{n}$) and, hence, larger CBP splittings; the maximal Berry flux is $\mathcal{F}_{\max} = m\mathcal{F}_{\text{single}}$. In such a structure, the long-range Coulomb interaction allows the photo excited densities in different layers to oscillate collectively.

Conclusion - CBPs are robust collective excitations of metallic systems, arising from two simple ingredients: Berry flux and interactions. Our analysis indicates CBPs survive for both weak and strong interactions. As a result, we conclude that CBPs are generic in metallic anomalous Hall phases, including out-of-equilibrium states where finite \mathcal{F} emerges from driving (e.g., in optically pumped valley polarization in Dirac materials). Indeed, this feature allows CBPs to be used for all-optical diagnostics of anomalous Hall and topological phases, as well as pumped or periodically driven systems e.g., Ref. [37, 38]. Optical probes of the latter are particularly appealing since transport measurements require contacts that often complicate and destroy the novel electron distributions and coherences of driven systems.

Perhaps the most appealing prospect, however, is coupling CBPs with light for sub-wavelength, and strong non-reciprocal propagation. Exhibiting a single chiral mode at large q (large splitting, and large frequency), precisely where plasmons give large compression of optical mode volume, hybrid CBP-polaritons are strongly non-reciprocal [17]. As we propose, CBP mediated unidirectional waveguides can be realized in readily available *non-magnetic* materials (e.g. the van der Waals material class). CBP based non-reciprocity, if realized experimentally, stands to play a vital role in the miniaturization of optical components that are magnetic field-free.

Acknowledgements - We thank J. Alicea, J. Eisenstein, M. Kats, L. Levitov, M. Schechter, and B. Skinner

for useful conversations. JS acknowledges support from the Walter Burke Institute for Theoretical Physics as part of a Burke fellowship at Caltech. MR acknowledges support from the Villum Foundation and the People Programme (Marie Curie Actions) of the European Union's Seventh Framework Programme (FP7/2007-2013) under REA grant agreement PIIF-GA-2013-627838.

[1] Nagaosa N., Sinova J., Onoda S., MacDonald A. H., Ong N. P., Anomalous Hall effect. *Rev Mod Phys* **82**, 1539-1592 (2010).

[2] Haldane F. D. M., Model for a Quantum Hall Effect without Landau Levels: Condensed-Matter Realization of the "Parity Anomaly," *Phys. Rev. Lett.* **61**, 2015 (1988).

[3] Yu R., et al, *Science* **329**, 61 (2010).

[4] Nomura K., Nagaosa N., *Phys. Rev. Lett.* **106**, 166802 (2011).

[5] Chang C.-Z., et al., Experimental Observation of the Quantum Anomalous Hall Effect in a Magnetic Topological Insulator, *Science* **34**, 1629 (2013)

[6] Wang Q.-Z., Liu X., Zhang H. Z., Samarth N., Zhang S.-C., Liu C.-X., Quantum Anomalous Hall Effect in Magnetically Doped InAs/GaSb Quantum Wells, *Phys. Rev. Lett.* **113**, 147201 (2014).

[7] Mak K. F., McGill K. L., Park J., McEuen P. L., The valley Hall effect in MoS₂ transistors. *Science* **344**, 1489-1492 (2014).

[8] Xiao D., Meng M. C., Niu Q., Berry phase effects on electronic properties, *Rev. Mod. Phys.* **82**, 1959-2007 (2010).

[9] Hasan M. Z., Kane C. L., Colloquium: Topological insulators. *Rev. Mod. Phys.* **82**, 3045 (2010).

[10] Allen S. J., Störmer H. L., Hwang J. C. M., Dimensional resonance of the two-dimensional electron gas in selectively doped GaAs/A₁GaAs heterostructures, *Phys. Rev. B*, **28** 4875 (1983).

[11] See e.g. Theis T. N., Plasmons in inversion layers, *Surf. Sci.* **98**, 515 (1980). D. Heitman, Two-dimensional plasmons in homogeneous and laterally microstructured space charge layers, *Surf. Sci.*, **170**, 332 (1986).

[12] Mast D. B., Dahm A. J., Fetter A. L., Observation of Bulk and Edge Magnetoplasmons in a Two-Dimensional Electron Fluid, *Phys. Rev. Lett.* **54**, 1706 (1985).

[13] Glattli D. C., Andrei E. Y., Deville G., Poitrenaud J., Williams F. I. B., Dynamical Hall Effect in a Two-Dimensional Classical Plasma, *Phys. Rev. Lett.*, **54**, 1710 (1985).

[14] See e.g. Kohn W., Cyclotron Resonance and de Haas-van Alphen Oscillations of an Interacting Electron Gas, *Phys. Rev.* **123** 1242 (1961); Brey L., Johnson N. F., Halperin B. I., Optical and magneto-optical absorption in parabolic quantum wells, *Phys. Rev. B* **40**, 10647-10649 (1989); Maksym P. A., Chakraborty, T., Quantum dots in a magnetic field: Role of electron-electron interactions, *Phys. Rev. Lett.* **65**, 108 (1990).

[15] Fetter A. L., Edge magnetoplasmons in a bounded two-dimensional electron fluid, *Phys. Rev. B* **32** 7676 (1985).

[16] Henriksen E. A., et al., Interaction-Induced Shift of the Cyclotron Resonance of Graphene Using Infrared Spectroscopy, *Phys. Rev. Lett.* **104** 067404 (2010).

[17] Jalas D., et al., What is - and is not- an optical isolator, *Nat. Photonics* **7**, 579 (2013).

[18] Barnes W. L., Dereux A., Ebbesen T. W., Surface plasmon subwavelength optics, *Nature* **424**, 828 (2003).

[19] Tame M. S., McEnery K. R., zdemir K., Lee J., Maier S. A., Kim M. S., Quantum Plasmonics, *Nat. Phys.* **9**, 329 (2013).

[20] Grigorenko A. N., Polini M., Novoselov K. S., Graphene Plasmonics, *Nat. Photonics* **6**, 749 (2012).

[21] Lifshitz E. M., Pitaevskii L. P., Physical Kinetics, *Butterworth-Heinemann* (1981).

[22] See Supplementary Online Information for a discussion of Euler equations and the kinetic equation, constitutive relations, and chiral Berry plasmon dipole modes in a disk, and photo-induced chiral Berry plasmons.

[23] Yoon H., et al., Measurement of collective dynamical mass of Dirac fermions in graphene. *Nat. Nano.* **9**, 594-599 (2014).

[24] Fetter A. L., Edge magnetoplasmons in a two-dimensional electron fluid confined to a half-plane, *Phys. Rev. B* **33**, 3717 (1986).

[25] Wang W., Apell P., Kinaret J., Edge plasmons in graphene nanostructures, *Phys. Rev. B* **84**, 085423 (2011).

[26] Price H. M., Cooper N. R., Effects of Berry Curvature on the Collective Modes of Ultracold Gases, *Phys. Rev. Lett.* **111**, 220407 (2013).

[27] Yan H., Li Z., Li X., Zhu W., Avouris P., Xia F., Infrared Spectroscopy of Tunable Dirac Terahertz Magnetoplasmons in Graphene, *Nano Lett.* **12**, 3766 (2012).

[28] Culcer D., MacDonald A., Niu Q., Anomalous Hall effect in paramagnetic two-dimensional systems, *Phys. Rev. B* **68**, 045327 (2003).

[29] Jones A. M., et al. Optical generation of excitonic valley coherence in monolayer WSe₂, *Nat. Nano.* **8**, 634-638 (2013).

[30] Ruppert C., Aslan O. B., Heinz T. F., Optical Properties and Band Gap of Single-and Few-Layer MoTe₂ Crystals, *Nano Lett.* **14**, 6231-6236(2014).

[31] Hunt B., et al., Massive Dirac Fermions and Hofstadter Butterfly in a van der Waals Heterostructure. *Science* **340**, 1427 (2013).

[32] Woods C. R., et al., Commensurate-incommensurate transition in graphene on hexagonal boron nitride, *Nat. Phys.* **10**, 451-456 (2014).

[33] Gorbachev R. V., et al., Detecting Topological Currents in Graphene Superlattices, *Science* **346**, 448 (2014).

[34] Zhang Y., Tang T.-T., Girit C., Hao Z., Martin M. C., Zettl A., Crommie M. F., Ron Shen Y., Wang F., Direct observation of a widely tunable bandgap in bilayer graphene, *Nature* **459**, 820-823 (2009).

[35] Yu H., Liu G.-B., Gong P., Xu X., Yao W., Dirac cones and Dirac saddle points of bright excitons in monolayer transition metal dichalcogenides, *Nat. Comm.* **5**, 3876 (2014).

[36] Lensky Y. D., Song J. C. W., Samutpraphoot P., Levitov L. S., Topological Valley Currents in Gapped Dirac Materials, *Phys. Rev. Lett.*, in press (2015).

[37] Yao W., MacDonald A. H., Niu Q., Optical Control of Topological Quantum Transport in Semiconductors, *Phys. Rev. Lett.* **99**, 047401 (2007).

[38] Kitagawa T., Oka T., Brataas A., Fu L., Demler E., Transport properties of nonequilibrium systems under the application of light: Photoinduced quantum Hall insulators without Landau levels, *Phys. Rev. B* **84**, 235108

(2011).

[39] We note that Kohn's theorem guarantees that splittings are unchanged for parabolic bands; weak renormalizations are expected for linearly dispersing systems such as graphene, where it has been measured to be at most of order 10%, see e.g., Ref. [16]. In contrast, for CBPs the splitting grows directly proportional with interaction strength [see Eq. (3) of the main text].

[40] The Berry curvature $\Omega(\mathbf{p}) = \nabla_{\mathbf{k}} \times \mathbf{A}_{\mathbf{k}}$ depends on the crystalline Bloch wavefunctions $|u_{\mathbf{k}}\rangle$, where $\mathbf{A}_{\mathbf{k}} = \langle u_{\mathbf{k}} | i \nabla_{\mathbf{k}} | u_{\mathbf{k}} \rangle$ is the Berry connection.

[41] Comparing this estimate to plasmon frequencies obtained in graphene disks (e.g., in Ref. [27]) we obtain zero field plasmon frequencies in the disk geometry to within a factor of unity. Using parameters reported in Ref. [27], our estimate yields $\hbar\omega_0 \approx \sqrt{2\pi e^2 n_0 / (md)} \approx 24$ meV for a disk of $d = 3 \mu\text{m}$ and doping reported $\mu = -0.54$ eV. Ref. [27] observed a zero field plasmon resonance at $\omega_0 = 130 \text{ cm}^{-1} = 16$ meV.

[42] The latter condition is important in TMDs e.g. MoS₂, since electronically coupled double MoS₂ layer restores inversion symmetry and does not exhibit a Berry curvature in its Bloch bands.

SUPPLEMENTARY ONLINE INFORMATION

For the convenience of the reader, in this supplement we provide a derivation of the Euler equations, including the role of anomalous velocity. We start from a general kinetic equation framework, giving a detailed derivation of the constitutive relations, a description of the matching matrix for edge CBPs, a full analysis of CBP dipole modes in a disk geometry, and analyze an example of “on-demand” CBPs in non-magnetic materials in valley polarized Dirac materials.

Euler equations and the kinetic equation

To analyze the collective modes of an electron liquid with nonvanishing Berry curvature we will employ a microscopic approach based on the quantum kinetic equation. The kinetic equation for the electronic distribution function $f_i(\mathbf{x}, \mathbf{p}, t)$ reads

$$(\partial_t + \mathbf{v} \nabla_{\mathbf{x}} + e \mathbf{E} \nabla_{\mathbf{p}}) f_i(\mathbf{x}, \mathbf{p}, t) = I^N + I^{\text{el-ph}} + I^{\text{dis}}, \quad (\text{S-1})$$

where \mathbf{E} is the electric field, i is the band index, and I^N , $I^{\text{el-ph}}$, I^{dis} describe (normal) two-particle collisions, electron-phonon collisions and scattering by disorder. The electric field can be either extrinsic (imposed externally) or intrinsic, arising due to long-wavelength charge fluctuations (as will be the case in our analysis of plasmons). Importantly, the velocity is given by Eq. (S-2) below, which accounts for both the “conventional” group velocity and Berry curvature induced anomalous velocity.

We will concentrate on the *hydrodynamical* regime, when the processes $I^{\text{el-ph}}$ and I^{dis} are negligible

($I^{\text{el-ph}}, I^{\text{dis}} \ll I^N$). Using the fact that the collision operator I^N conserves particle number, momentum, and energy of the electron liquid, we can obtain a hydrodynamic description of momentum, and particle transport. Integrating Eq.(S-1) over \mathbf{p} yields the continuity equation for particle number; multiplying Eq.(S-1) by \mathbf{p} , and subsequently integrating and accounting for energy and momentum conservation by interparticle collisions, yields equations for momentum transport. Thus we obtain the Euler equations shown in Eq. (1) of the main text.

Constitutive Relations

The anomalous constitutive relation in Eq. (2) of the main text emerges from the microscopics of electron motion in materials with non-vanishing Berry curvature, $\Omega(\mathbf{p})$. Carrier dynamics of quasiparticles possessing Berry curvature are encoded by the semi-classical equations of motion for electrons [8]

$$\mathbf{v}_{\mathbf{p}} = \frac{\partial \varepsilon_{\mathbf{p}}}{\partial \mathbf{p}} + \frac{1}{\hbar} \dot{\mathbf{p}} \times \Omega(\mathbf{p}), \quad \dot{\mathbf{p}} = e \nabla \phi(\mathbf{x}), \quad (\text{S-2})$$

where, $\mathbf{v}_{\mathbf{p}} = \dot{\mathbf{x}}$ is the electron velocity, $\varepsilon_{\mathbf{p}}$ is the Bloch band dispersion, and $-e < 0$ is the electron charge. The Berry curvature, given by $\Omega(\mathbf{p}) = \nabla_{\mathbf{k}} \times \mathbf{A}_{\mathbf{k}}$, is an intrinsic property of Bloch wave functions in certain crystals, with the Berry connection defined as $\mathbf{A}_{\mathbf{k}} = \langle u_{\mathbf{k}} | i \nabla_{\mathbf{k}} | u_{\mathbf{k}} \rangle$, where $|u_{\mathbf{k}}\rangle$ is the Bloch function. For the 2D systems considered in this work, $\Omega = \Omega \hat{\mathbf{z}}$.

Taking phase space averages of the semiclassical equations of motion in Eq. (S-2), using $\bar{\mathcal{O}} = \sum_{\mathbf{p}, i} \mathcal{O} f_i(\mathbf{x}, \mathbf{p}, t)$ with $\mathcal{O} = \mathbf{v}, \mathbf{p}$, yields the constitutive relations. Here $f_i(\mathbf{x}, \mathbf{p}, t)$ is the full phase space distribution of the carriers in each of the bands i . The stress tensor is expressed as $\bar{\sigma}_{ij} = \bar{v}_i \bar{p}_j$, and the electron density is given by $n(\mathbf{x}, t) = \sum_{\mathbf{p}, i} f_i(\mathbf{x}, \mathbf{p}, t)$. We evaluate these quantities below.

In the hydrodynamic regime, where collisions are dominated by electron-electron scattering, we write the distribution function as [21]

$$f_i(\mathbf{x}, \mathbf{p}, t) = \frac{1}{e^{\beta(\varepsilon_{\mathbf{p}}^i - \mathbf{p} \cdot \mathbf{u}(\mathbf{x}, t) - \mu(\mathbf{x}, t))} + 1}. \quad (\text{S-3})$$

The equation above determines the \mathbf{x} and \mathbf{p} dependence of the phase space distribution in terms of the free space and time dependent fields \mathbf{u} , β and μ . Here $\mathbf{u}(\mathbf{x}, t)$ generates a collective momentum shift for the electron fluid, $\beta(\mathbf{x}, t)$ describes temperature variations, and $\mu(\mathbf{x}, t)$ describes the local chemical potential deviation from equilibrium. Note that completely filled bands are irrelevant for describing the momentum and stress densities. However, as we show below, the velocity field $\bar{\mathbf{v}}$ is sensitive to the filling of all lower bands.

For weak inhomogeneity, and focusing on the bulk, we write $f(\mathbf{x}, \mathbf{p}, t) = f_0(\mathbf{p}) + \delta f(\mathbf{x}, \mathbf{p}, t)$, where $f_0(\mathbf{p}) =$

$(e^{\beta(\varepsilon_{\mathbf{p}} - \mu)} + 1)^{-1}$ is the equilibrium distribution. Using Eq. (S-3), this gives

$$\delta f = \left(\frac{\varepsilon - \mu}{\beta} \delta\beta - \delta\mu \right) \frac{\partial f_0}{\partial \varepsilon} - \mathbf{u} \cdot \mathbf{p} \frac{\partial f_0}{\partial \varepsilon}. \quad (\text{S-4})$$

This relation allows the quantities $\bar{\mathbf{p}}, \bar{\mathbf{v}}, \bar{\sigma}_{ij}$ in Eq. (1) of the main text to be expressed in terms of the fields $\mathbf{u}, \delta\beta$, and $\delta\mu$. For ease of notation, we will denote the term in the first parenthesis as $\delta_1 f$.

Using Eq. (S-4) and keeping terms up to linear order in δf , we write

$$\bar{\mathbf{p}}(\mathbf{x}, t) = A\mathbf{u}, \quad \frac{\partial \varepsilon}{\partial \mathbf{p}} = B\mathbf{u}, \quad (\text{S-5})$$

where

$$A = \frac{1}{2} \sum_{\mathbf{p}} |\mathbf{p}|^2 \left(-\frac{\partial f}{\partial \varepsilon} \right), \quad B = \frac{1}{2} \sum_{\mathbf{p}} \left[\frac{\partial \varepsilon}{\partial \mathbf{p}} \cdot \mathbf{p} \right] \left(-\frac{\partial f}{\partial \varepsilon} \right). \quad (\text{S-6})$$

We note that the $\bar{\mathbf{p}}$ and $\bar{\mathbf{v}}$ depend only on the anisotropic part of δf , captured by \mathbf{u} . This is because \mathbf{p} and \mathbf{v} integrated using $\sum_{\mathbf{p}} \mathcal{O} \delta_1 f$ yields a vanishing result (the same is true for integral over f_0); here $\mathcal{O} = \mathbf{p}, \mathbf{v}$. Similarly, we find the anomalous velocity contribution, $\bar{\mathbf{v}}_a$ is

$$\bar{\mathbf{v}}_a = \frac{1}{\hbar} \sum_{\mathbf{p}, i} [e \nabla \phi \times \Omega_i(\mathbf{p})] f_i(\mathbf{x}, \mathbf{p}, t) \approx \frac{e \mathcal{F}}{\hbar} [(\nabla \phi) \times \hat{\mathbf{z}}], \quad (\text{S-7})$$

where $\mathcal{F} = \sum_{\mathbf{p}, i} \Omega_i(\mathbf{p}) f_i^{\text{eq}}(\mathbf{p})$, and $f_i^{\text{eq}}(\mathbf{p}) = f_0$ is the Fermi-Dirac distribution. Here, we have only kept terms linear in δf , and noted that ϕ is proportional to δf (see below).

Combining Eqs. (S-6) and (S-7) we obtain the anomalous constitutive relation in Eq. (2) of the main text, with $m = A/B$. The mass associated with the collective plasmonic mode, $m = A/B$, does not need to be the same as the single particle mass. Indeed, for the *massless* Dirac system graphene, a finite collective mass has been measured [23]. In the degenerate limit $\beta\mu \gg 1$, the plasmon mass is $m = p_F/v_F$, where p_F is the Fermi momentum, and v_F is the Fermi velocity [23]. For a gapped Dirac system with dispersion $\varepsilon = \sqrt{v_F^2 p^2 + \Delta^2}$, we obtain $m = \sqrt{v_F^2 p_F^2 + \Delta^2}/v^2 = \mu/v_F^2$ for $(\mu \geq \Delta)$.

In the same fashion as above, we find that density and the stress tensor depend only on the isotropic part of δf , encoded in $\delta\beta$ and $\delta\mu$, as

$$\delta n = a_1 \delta\beta + a_2 \delta\mu, \quad \sigma_{ij} = \delta_{ij} [b_1 \delta\beta + b_2 \delta\mu], \quad (\text{S-8})$$

where $a_1 = \sum_{\mathbf{p}} \frac{\partial f}{\partial \varepsilon} \frac{\varepsilon - \mu}{\beta}$, $a_2 = \sum_{\mathbf{p}} \frac{\partial f}{\partial \varepsilon}$, and $b_1 = \sum_{\mathbf{p}} \frac{\partial \varepsilon}{\partial \mathbf{p}} \cdot \mathbf{p} \frac{\partial f}{\partial \varepsilon}$, $b_2 = \sum_{\mathbf{p}} \frac{\partial \varepsilon}{\partial \mathbf{p}} \cdot \mathbf{p} \frac{\partial f}{\partial \varepsilon}$. We note that since \mathbf{v} contains the anomalous velocity, the stress tensor can in principle depend on the anomalous velocity via

$$\sigma_{ij}^a = \sum_{\mathbf{p}} (e \nabla \phi \times \hat{\mathbf{z}}) \cdot \mathbf{p}_j \Omega(\mathbf{p}) (f_0 + \delta_1 f), \quad (\text{S-9})$$

where we have denoted the anomalous velocity contribution by the superscript a . Taking a minimal model for finite Berry flux (i.e., with time reversal symmetry broken, but inversion symmetry preserved), we have $\Omega(\mathbf{p}) = \Omega(-\mathbf{p})$ [8]. As a result, the summand in Eq. (S-9) is odd in \mathbf{p} and the sum vanishes.

We note parenthetically that the stress tensor drops out in the analysis of CBP dipole modes, see main text and section below in supplementary information. Furthermore, we note that higher order contributions, e.g., viscous terms [21], can also contribute to the stress tensor. However, their influence is expected to be small and we neglect them in our treatment; including these terms into an analysis of particle transport is a subject of current research interest [S1]. In the degenerate limit $\beta\mu \gg 1$, Eq. (S-8) reduces to $\sigma_{ij} = \frac{\mu}{2} \delta_{ij} \delta n$. The factor of 1/2 comes from an angular average and is related to the dimensionality $d = 2$.

Using these constitutive relations, i.e., Eq. (2) of the main text along with $\sigma_{ij} = \frac{\mu}{2} \delta_{ij} \delta n$, and writing $\mathbf{E} = -\nabla_{\mathbf{x}} \int d\mathbf{x}' \frac{e}{\kappa |\mathbf{x} - \mathbf{x}'|} \delta n(\mathbf{x}', t)$, we now look for travelling wave solutions $\sim e^{i\mathbf{q} \cdot \mathbf{r} - i\omega t}$ in the *bulk*. Seeking zero-modes of the Euler equations [Eq. (1) of the main text] gives

$$(\omega_{\mathbf{q}}^{\text{bulk}})^2 = 2\pi n_0 e^2 |\mathbf{q}| B / (\kappa A) + |\mathbf{q}|^2 (B\mu/2A), \quad (\text{S-10})$$

where κ is the background dielectric constant. The first term is associated with interactions, and the second term is associated with compressional sound modes arising from the stress density of the electron liquid [15, 24] [S2].

To clarify the physical dependence on parameters, it is useful to non-dimensionalize Eq. (S-10) by multiplying through by \hbar^2/μ^2 . This yields Eq. (5) of the main text (reproduced here for convenience) with

$$(\hbar\omega_{\mathbf{q}}^{\text{bulk}}/\mu)^2 = a_0 (|\mathbf{q}|/q_0) + (|\mathbf{q}|/q_0)^2, \quad (\text{S-11})$$

where a_0 is dimensionless and q_0 is a characteristic inverse scale (associated with the compressional wave):

$$a_0 = \frac{4\pi e^2 n_0}{\kappa \mu q_0}, \quad q_0^2 = \frac{2A\mu}{B\hbar^2}. \quad (\text{S-12})$$

For a gapped Dirac system with N species of fermions, $n_0 = N\mu^2/(4\pi\hbar^2 v_F^2)$ and $A/B = m = \mu/v_F^2$ yielding $q_0 = \sqrt{2\mu}/(v_F \hbar) \approx 2.15 \times (\mu[\text{meV}]) \times 10^4 \text{ cm}^{-1}$ and $a_0 = Ne^2/(\sqrt{2}\kappa v_F \hbar)$. In the latter expression, setting $N = 4$, dielectric constant $\kappa = 1$, and using $v_F = 10^8 \text{ cm/s}$, we obtain $a_0 \approx 6.2$.

Matching matrix for edge CBPs

The edge CBPs shown in Figs. 1 and 2 were obtained from the localized modes in Eq. (6), which solve Eq. (4) while satisfying the boundary conditions: ϕ and $\partial_x \phi$ continuous across the boundary ($x = 0$), and \bar{v}_x vanishing at

$x = 0$. Crucially, \bar{v}_x depends on the Berry Flux, \mathcal{F} . The boundary conditions can be compactly expressed via the relation $\mathcal{S}\Phi = 0$, where $\Phi = (\phi_0, \phi_1, \phi_2)^T$ and

$$\mathcal{S} = \begin{pmatrix} 1 & -1 & -1 \\ \sqrt{2}|\tilde{q}| & \tilde{\gamma}_1 & \tilde{\gamma}_2 \\ 0 & D_1 & D_2 \end{pmatrix}. \quad (\text{S-13})$$

Here $D_{1,2} = \tilde{\gamma}_{1,2}[\tilde{\gamma}_{1,2}^2 - 2\tilde{q}^2 - 2\tilde{\omega}_{\mathbf{q}}^2] + \text{sgn}(q)C\tilde{\omega}_{\mathbf{q}}\tilde{q}^2$, and we have used non-dimensionalized quantities so that $C = 4\pi e^2 \mathcal{F} q_0 / (\mu\kappa)$, $\tilde{\gamma}_{1,2} = \gamma_{1,2}/q_0$, $\tilde{q} = q/q_0$, and $\tilde{\omega}_{\mathbf{q}} = \hbar\omega_{\mathbf{q}}/\mu$ [see Eq. (5)]. Edge CBPs are identified through zero modes of the matrix in Eq. (S-13), as plotted as blue and red curves in Figs. 1,2. In all plots, we use $\kappa = 1$.

CBP dipole mode in a disk

Here we present a more complete analysis of the CBP dipole modes in a disk, which dominate the optical absorption in metallic disks. These dipole modes can be conveniently described through the center of mass (COM) motion, $\{\mathbf{x}(t)\}$, wherein all internal forces cancel (viz. Newton's third law). Here $\{\cdot\}$ denotes the COM average, with $\{\mathbf{x}(t)\} = \int d^2\mathbf{x} n(\mathbf{x}, t)\mathbf{x}$, and $\{\mathbf{p}(t)\} = \int d^2\mathbf{x} \bar{\mathbf{p}}(\mathbf{x}, t)$. The COM equations of motion can be obtained from Eq. (1) of the main text via integration by parts, along with the condition that the velocity and stress density vanish when $|\mathbf{x}| \rightarrow \infty$. This yields

$$\partial_t\{\mathbf{x}\} = \left\{ \frac{\partial \varepsilon}{\partial \mathbf{p}} \right\} + \frac{1}{\hbar} \{e\nabla\phi \times \boldsymbol{\Omega}(\mathbf{p})\}, \quad \partial_t\{\mathbf{p}\} = \{e\nabla\phi\}, \quad (\text{S-14})$$

where \mathbf{E} is a self-generated electric field associated with the plasmon motion.

To capture the dipolar mode, we use the harmonic potential $-e\phi(\mathbf{x}) = \frac{m}{2}\omega_0^2|\mathbf{x}|^2$ for the electrons (see e.g., Ref. [27]) where ω_0 is the bare plasmon frequency in a disk (with diameter d) in the *absence* of Berry curvature.

In analyzing the COM equations of motion, we first note that $e\nabla\phi(\mathbf{x})$ depends only on \mathbf{x} , and $\boldsymbol{\Omega}(\mathbf{p})$ only on \mathbf{p} . Keeping terms to linear order in δn , we find the anomalous velocity contribution $\{\mathbf{v}_a\}$ for the COM as

$$\begin{aligned} \{e\nabla\phi \times \boldsymbol{\Omega}\} &= \sum_{\mathbf{x}} \left[e\nabla\phi(\mathbf{x}) \times \sum_{\mathbf{p}, i} \boldsymbol{\Omega}(\mathbf{p}) f_i(\mathbf{x}, \mathbf{p}, t) \right] \\ &= \left[\sum_{\mathbf{x}} e\nabla\phi(\mathbf{x}) \mathcal{F}(\mathbf{x}, t) \right] \times \hat{\mathbf{z}} \approx \zeta \{\mathbf{x}(t)\} \times \hat{\mathbf{z}}, \end{aligned} \quad (\text{S-15})$$

where the Berry flux is given by $\mathcal{F}(\mathbf{x}, t) \equiv \sum_{\mathbf{p}, i} \Omega_i(\mathbf{p}) f_i(\mathbf{x}, \mathbf{p}, t)$, the constant ζ can be obtained as detailed below, and i is a band index. Here we will concentrate on the motion of bulk electrons in a given band, n . We therefore take $f_{i < n} = 1$ everywhere inside the disk for bands below n (but vanishing outside

the disk). Under the assumption of local equilibrium, we set $f_n(\mathbf{x}, \mathbf{p}, t) = [e^{\beta(\varepsilon_{\mathbf{p}}^n - \mu(\mathbf{x}, t))} + 1]^{-1}$, where $\mu(\mathbf{x}, t)$ is a space and time varying chemical potential. Adopting a simple model of a rigidly moving disk of charge with constant density n_0 , and density equal to zero outside, gives $\mathcal{F} = \mathcal{F}n(\mathbf{x}, t)/n_0$ and $\zeta = -\frac{\mathcal{F}}{n_0} m \omega_0^2$. Here \mathcal{F} is obtained with a fixed uniform chemical potential μ .

Using $\{e\nabla\phi\} = -m\omega_0^2\{\mathbf{x}(t)\}$, Eq. (S-15), and substituting into Eq. (S-14), we obtain the equations of motion for the dipole mode: $(\partial_t^2 + A_{ij})\{\mathbf{x}_j\} = 0$, where

$$\mathbf{A} = \begin{pmatrix} \omega_0^2 & \omega_a \partial_t \\ -\omega_a \partial_t & \omega_0^2 \end{pmatrix}, \quad \omega_a = \frac{\mathcal{F}\omega_0^2 m}{n_0 \hbar}. \quad (\text{S-16})$$

Here we have written $\left\{ \frac{\partial \varepsilon}{\partial \mathbf{p}} \right\} = \frac{1}{m}\{\mathbf{p}\} + \mathcal{O}(\delta n^2)$ and kept only terms up to linear order in δn .

Writing $\{\mathbf{x}\} = \mathbf{x}_0 e^{i\omega t}$, we obtain a secular equation $\mathbf{M}\mathbf{x}_0 = 0$ where \mathbf{M} is obtained from \mathbf{A} by replacing ∂_t by $i\omega$. Plasmons are given by the zero modes, $\det(\mathbf{M}) = 0$, yielding the split dispersion relation

$$\omega_{\pm} = \sqrt{\omega_0^2 + \frac{\omega_a^2}{4}} \pm \frac{\omega_a}{2}, \quad (\text{S-17})$$

where $\omega_{\pm}, \omega_0 > 0$ (in the following we will use only positive frequencies; a similar analysis yields the same results for negative ω_{\pm}, ω_0 as well). These plasmon modes are *chiral* as they correspond to a rotating COM displacement and momentum

$$\{\mathbf{x}(t)\}_{\pm} = \frac{|\mathbf{x}_0|}{\sqrt{2}} \begin{pmatrix} 1 \\ \pm i \end{pmatrix} e^{i\omega_{\pm} t}, \quad \{\mathbf{p}(t)\}_{\pm} = \frac{i\omega_0^2 m}{\omega_{\pm}} \{\mathbf{x}(t)\}, \quad (\text{S-18})$$

where $\{\mathbf{p}(t)\}_{\pm}$ and $\{\mathbf{x}(t)\}_{\pm}$ are offset by a phase of $\pi/2$. As a result, a rotating $\{\mathbf{x}(t)\}_{\pm}$ gives rise to a circulating momentum/current density (see Fig. 3a of the main text). The clockwise/anticlockwise (ω_+/ω_-) motion of chiral plasmons sketched in Fig. 3a are oriented for a positive Berry flux, \mathcal{F} , pointing in the $\hat{\mathbf{z}}$ direction. This direction sets the orientation of ω_a . For opposite sign of \mathcal{F} the orientations are switched. The distinct frequencies ω_{\pm} arise from the anomalous velocity $\{\mathbf{v}_a\}$ adding/subtracting propagation speed from the modes at $\mathcal{F} = 0$.

The CBP dipole mode can manifest in distinct split peaks for optical absorption. This splitting can be analyzed by writing the current density as $\mathbf{j} = n_0 e \partial_t \{\mathbf{x}\}$ by inverting Eq. (S-16), and relating current to electric field via $\mathbf{j} = \mathbf{g}\mathbf{E}$, where \mathbf{E} is probing field, and \mathbf{g} is the conductivity tensor. Optical absorption is characterized by the real part of the longitudinal conductivity, \mathbf{g}_{xx} , as

$$\text{Re}[g_{xx}(\omega)] = \frac{1}{2} \sum_{\pm} \frac{\mathcal{D}\Gamma\omega^2}{(\omega^2 \pm \omega\omega_a - \omega_0^2)^2 + \Gamma^2\omega^2}, \quad (\text{S-19})$$

where $\mathcal{D} = \frac{n_0 e^2}{m}$ is the Drude weight, and Γ is the transport relaxation rate, included phenomenologically

via $\partial_t^2 \rightarrow \partial_t^2 + \Gamma \partial_t$. This yields the split peak optical absorption for the disk geometry shown in Fig. 3b of the main text.

Optically pumped “On-Demand” CBP dipole mode in gapped Dirac materials

Here we consider how CBPs might arise in non-magnetic gapped Dirac materials such as MoS₂, or gapped G/h-BN. To analyze this, we focus on nominally time reversely invariant gapped Dirac materials. We model the valley dependent \mathcal{F} as [36]: $\mathcal{F}_{K,K'} = \tau_z N_s \frac{\tilde{n}^{1/2}}{2(n_{K,K'} + \tilde{n})^{1/2}} \text{sgn } \Delta$, where $n_{K,K'}$ are the valley carrier densities, $\tau_z = \mp$ for the K, K' valleys, $N_s = 2$ is the spin degeneracy, and $\tilde{n} = \Delta^2/4\pi v_F^2 \hbar^2$ gives a characteristic density scale. The bandgap is $2|\Delta|$. When $n_K = n_{K'}$, the total flux $\mathcal{F} = \mathcal{F}_K + \mathcal{F}'_K$ vanishes.

However, a non-vanishing net Berry flux \mathcal{F}_{pe} for the photoexcited system is achieved when $n_K \neq n_{K'}$ (Fig. 3c inset). Setting $n_{K'} = 0$, giving $\mathcal{F}_{K'} = +1$, the valley polarized electron (n_{el}) and hole (n_{h}) populations concentrated at the K valley conduction and valence band extrema yield

$$\begin{aligned} \mathcal{F}_{\text{pe}} &\approx 1 - \frac{1}{2} \left[\frac{\tilde{n}^{1/2}}{\sqrt{\tilde{n} + n_{\text{h}}}} + \frac{\tilde{n}^{1/2}}{\sqrt{\tilde{n} + n_{\text{el}}}} \right], \\ \tilde{n} &= 1.8 \times 10^{13} \frac{(\Delta[\text{eV}])^2}{(v_F[\text{cm s}^{-1}]/10^8)^2} \text{cm}^{-2}. \end{aligned} \quad (\text{S-20})$$

Here we have used that Berry curvature (including its sign) is the same for electrons and holes, following from particle-hole symmetry of the Dirac Hamiltonian, and used the convention $n_{\text{el,h}} > 0$. In deriving Eq. (S-20), we used the spin degeneracy $N_s = 2$ for the K' valley, and noted that only a single spin species in the K valley is excited by the circularly polarized light.

For demonstration we examine CBPs in the disk geometry as above. We analyze the coupled motion of photoexcited electrons and holes in a single valley via COM coordinates ($\{\mathbf{x}_{\text{el}}\}$) and ($\{\mathbf{x}_{\text{h}}\}$), respectively, giving:

$$\left[\partial_t^2 + \begin{pmatrix} \mathbf{A}_{\text{el}} & -\mathbf{A}_{\text{el}} \\ -\mathbf{A}_{\text{h}} & \mathbf{A}_{\text{h}} \end{pmatrix} \right] \begin{pmatrix} \{\mathbf{x}_{\text{el}}\} \\ \{\mathbf{x}_{\text{h}}\} \end{pmatrix} = 0, \quad (\text{S-21})$$

where \mathbf{A}_{el} and \mathbf{A}_{h} are defined as in Eq. (7) of the main text, with the density n_0 and plasmon mass m replaced by the appropriate values for electrons or holes. In writing these equations, we have used that the restoring force arising from the mutual attraction of photoexcited electron and hole subsystems is $\{e\nabla\phi\}_{\text{el(h)}} \approx \mp\alpha(\{\mathbf{x}_{\text{el}}\} - \{\mathbf{x}_{\text{h}}\})$, where $\{\cdot\}_{\text{el,h}}$ denote the COM averages for electron and hole distributions and the upper (lower) sign is for electrons (holes). Here α characterizes the strength of the electron-hole interaction. For brevity, in the following analysis we set $\mathbf{A}_{\text{el}} = \mathbf{A}_{\text{h}}$, giving $\alpha = m\omega_0^2$, where ω_0 is the plasmon frequency associated with a unipolar system with carrier density $n = n_{\text{el}} = n_{\text{h}}$.

Zero modes of Eq. (S-21) with $\partial_t^2 \rightarrow -\omega^2$ yield CBPs with $\{\mathbf{x}_{\text{el}}\} = -\{\mathbf{x}_{\text{h}}\}$, giving:

$$\omega_{\pm}^{\text{el-h}} = \sqrt{\omega_a^2 + 2\omega_0^2} \pm \omega_a, \quad (\text{S-22})$$

where ω_a is given by Eq. (7) with \mathcal{F} replaced by \mathcal{F}_{pe} . Importantly, $\omega_{\pm}^{\text{el-h}}$ chiral (electron-hole) plasmons feature *co-rotating* $\{\mathbf{x}_{\text{el}}\}$ and $\{\mathbf{x}_{\text{h}}\}$. This dipole like rotation follows from the equal sign of \mathcal{F} for electrons and holes. Modes with $\{\mathbf{x}_{\text{el}}\} = \{\mathbf{x}_{\text{h}}\}$ are also eigenmodes of Eq. (S-21). However, they have frequency, $\omega = 0$.

S1. See e.g., D. T. Son, A. O. Starinets, Viscosity, Black Holes, and Quantum Field Theory, *Annual Reviews of Nuclear and Particle Science*, 57:95-118 (2007)
S2. Phan T. V., Song J. C. W., Levitov L.S., Ballistic Heat Transfer and Energy Waves in an Electron System, arXiv:1306.4972 (2013).